PHILIPPINE ENGINEERING JOURNAL
PEJ 2025; Vol. 46, No. 1: 66-87

*Received: 27 December 2024*
*Received in Revised Form: 9 March 2025*
*Accepted: 30 April 2025*

# Machine Learning-Based Estimation of Modal Properties of a Transmission Tower in Bataan, Philippines

***Roydon Jude S. Samudio* and Jaime Y. Hernandez Jr.***
*Institute of Civil Engineering, University of the Philippines Diliman, Quezon City, Philippines*
**Corresponding author: judesamudio2018@gmail.com*

***Abstract*** *– Although fully automated modal analysis, a Structural Health Monitoring (SHM) technique, has recently been used to monitor the current condition of various civil structures, its application to wind-sensitive transmission towers remains limited. Most modal analysis and dynamic characterization studies related to these towers, which are essential for first-level damage detection, still require manual selection of input parameter values. This paper aims to contribute to the existing discussion by applying a machine learning (ML) algorithm to Stochastic Subspace Identification (SSI) to derive the modal parameters of a transmission tower located in Orion, Bataan, Philippines, thereby enhancing existing methodologies. In addition to utilizing Random Forest as the core intelligence of the method, the research explores three other ML algorithms—XGBoost, Decision Trees, and k-Nearest Neighbors (KNN)—as alternative modal prediction models within the framework. Despite limitations in sensor placement—restricted to the tower's lower half—the study successfully extracted ten frequency values from an actual transmission tower, closely aligning with analytical predictions. The first mode from the field data was identified at 3.21 Hz, with only a 0.63% deviation from the analytical model. Damping ratios, ranging from 0.68% to 3.02%, exhibited deviations of up to 138% for the fundamental mode but remained within international code recommendations, such as the ASCE 74 guideline of 4%. Random Forest stands out among the ML models tested, showing the fastest runtime, highest performance accuracy, and smallest Coefficient of Variation (CoV) values given random datasets, closely followed by XGBoost. A variability analysis over 120 two-minute datasets showed frequency CoVs between 0.42% and 2.39%, and damping CoVs between 2.02% and 7.02%. The results of this study can be used in model updating and the structural design of transmission towers in the Philippines. They also serve as a baseline for future recordings, facilitating enhanced and data-driven post-disaster decision-making.*

***Keywords:*** *automated modal analysis, transmission tower, machine learning, structural health monitoring, modal parameters*

## I. INTRODUCTION

Many studies have highlighted the vulnerability of transmission towers and their critical role in a nation's economy [1, 2, 3], particularly for a disaster-prone country like the Philippines. Repairing power transmission lines incurs substantial costs, approximately one million dollars per kilometer [4], making the damage from these incidents seemingly irreversible [5, 6]. Despite their crucial function in sustaining power networks, transmission

towers remain an under-researched topic, particularly within the Philippines' engineering and infrastructure sector. A deeper understanding of their dynamic behavior will contribute to safer and more durable designs, ultimately improving long-term power grid reliability.

Over the years, researchers have investigated the dynamic characteristics of transmission towers, particularly their response to extreme wind conditions. Several experimental and numerical approaches have emerged, including wind tunnel tests for design validation [7], Finite Element Modeling (FEM) for structural modeling [8], and fragility and vulnerability assessments [9]. However, among these, Structural Health Monitoring (SHM) has gained the most attention due to its ability to provide real-time monitoring, early warning systems, and predictive maintenance strategies. Recent advancements in sensor technology and data-driven analysis have further reinforced the shift toward automated SHM of different structures, ensuring greater accuracy in detecting structural anomalies and improving long-term maintenance efficiency [10, 11, 12, 13, 14].

In the field of SHM, Operational Modal Analysis (OMA) has been widely adopted to estimate damage-sensitive features in structures using system identification techniques without requiring external excitation. Stochastic Subspace Identification (SSI) is particularly useful for handling large vibration datasets with high computational efficiency and automation potential [15, 16]. However, traditional SSI methods present several challenges [18]. One significant limitation is the misidentification of spurious modes as stable ones, especially when working with extensive datasets, despite the application of stabilization diagrams (SD) [19, 20]. This issue arises due to the nature of SSI's mathematical framework and the inherent noise present in vibration data. Additionally, SSI relies on the subjective selection of critical control parameters, such as the number of block rows ($i$) and system order ($n$). If these parameters are incorrectly set—either too high or too low—the method tends to produce unwanted modes and misidentify a structure's dynamic properties [21, 24].

Several studies have emphasized this challenge. Zini et al. [22] and Tronci et al. [23] highlighted that existing research has not fully addressed the automated selection of control parameters, particularly $i$ and $n$, leading to inconsistencies in modal identification. Similarly, Ardilla et al. (2023) noted that the exact system order is never precisely known, and current strategies often lead to overestimation or underestimation of modal parameters, affecting the reliability of the identification process. These limitations of traditional SSI techniques have been observed in recent OMA studies on transmission towers, including the works of Li et al. [25], Hsu et al. [26], Xingjie et al. [27], and Feng et al. [28]. Their findings highlight the need for enhanced automation, improved parameter selection strategies, and noise mitigation techniques to refine modal analysis accuracy for transmission towers.

To overcome parameter selection challenges, Zhou et al. [29] proposed a Monte Carlo-based technique, randomly sampling $i$ and $n$ values to optimize real-mode extraction. Given the large volume of outputs, machine learning (ML) was integrated to filter and analyze results from large-scale simulations. In 2023 [32], Zhou et al. further refined their approach using XGBoost (XG) and DBSCAN to automatically detect closely spaced modes and optimize parameter selection. Rosso et al. [30] expanded on Zhou et al.'s [29] work, still using a Monte Carlo approach but incorporating four control parameters, including time window length ($j$)

and time instant parameters ($t$), identifying their position within the monitored signal. Specifically, the study utilizes a Halton Technique to generate random sets of control parameters, removing the subjectivity currently faced by existing challenges. Given the large number of outputs, they used Random Forest (RF) to classify and predict feasible sets, aiming to estimate the physical modes. This method was validated on a high-rise tower in Kuwait, successfully estimating physical modes close to its analytical results. Cucuzza et al. [31] adapted the technique to extract the dynamic properties of two confined masonry buildings in Italy. While the RF method produced robust results, the literature did not explore the computational advantages of using RF compared to other learning methods.

Despite these advancements, few studies have validated ML-driven SSI for transmission towers. This study aims to contribute to the ongoing discussion on SHM for these structures by applying SSI using Rosso et al.'s open-source automated modal identification package. The study evaluates RF as the core intelligence while also exploring XG [29], Decision Trees (DT) [6, 47], and k-Nearest Neighbors (KNN) [48] as alternative models. This study integrates various SHM techniques [35, 36, 37] for data collection, preprocessing, and post-processing. The method is first applied to FEM-generated vibration data and then compares modal results extracted from the field. Additionally, modal parameters derived through Brincker and Andersen's SSI approach [33] and Caicedo et al.'s NExT-ERA method [34] serve as benchmarks for validation.

## II. DATA ACQUISITION AND PREPROCESSING

The data collection process in this study is structured into two main stages: the Pre-validation (PV) Stage, which involves computer-simulated responses, and the Field Implementation (FI) Stage, where real-world vibration data is collected from an actual transmission tower. Figure 1 presents the study framework, detailing the integration of these two data sources into the ML-based SSI approach.

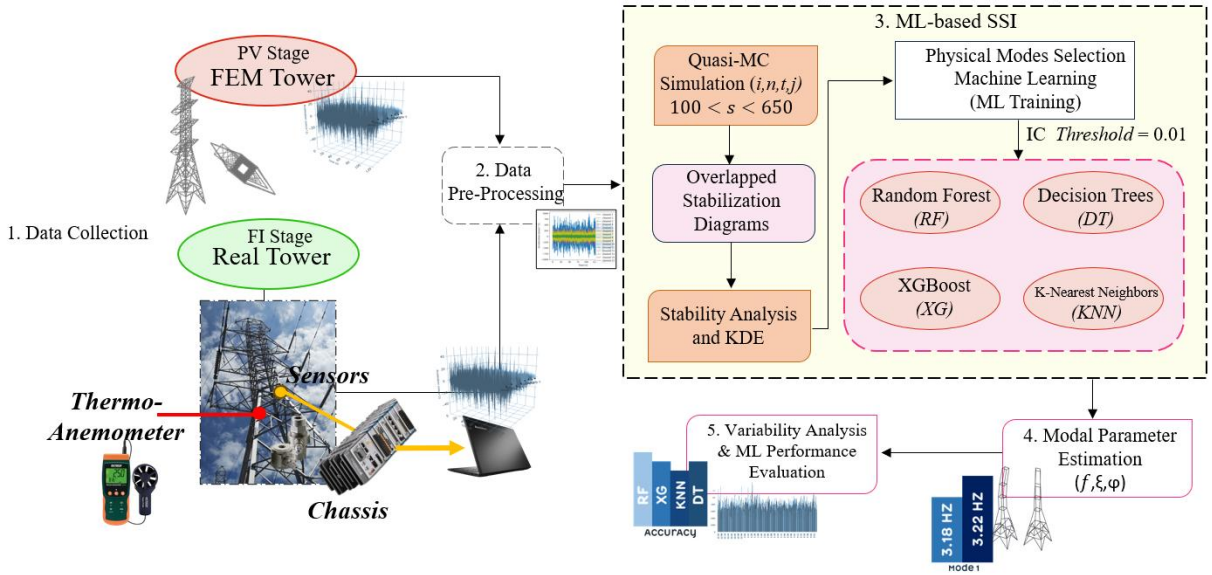


***Figure 1.*** Study framework.

In the PV Stage, an FEM of the transmission tower is developed using ETABS, and random excitation generated in MATLAB is applied to simulate structural responses. These digitally generated signals serve as a reference for validating the results obtained from field measurements.

For the FI Stage, field testing is conducted on a 230-kV steel lattice transmission tower operated by Peninsula Electric Cooperative, Incorporated (PENELCO) in Orion, Bataan, Philippines. The tower stands 38 meters tall, featuring a tapered cross-section with a base leg width of 7 meters, gradually reducing to 2.5 meters at 17.8 meters above ground. The field monitoring system, as shown in Figure 2, consists of 16 wired accelerometers installed at three distinct heights (5 m, 10 m, and 17.8 m), a thermo-anemometer for recording wind conditions, data acquisition devices, and a power supply. Vibration measurements were conducted in February 2024, coinciding with a scheduled power interruption by PENELCO to ensure safe and uninterrupted data collection. The total field test duration was approximately nine hours, including scaffolding setup, with four hours dedicated to continuous vibration monitoring. Wind-induced excitation served as the sole source of structural vibrations.

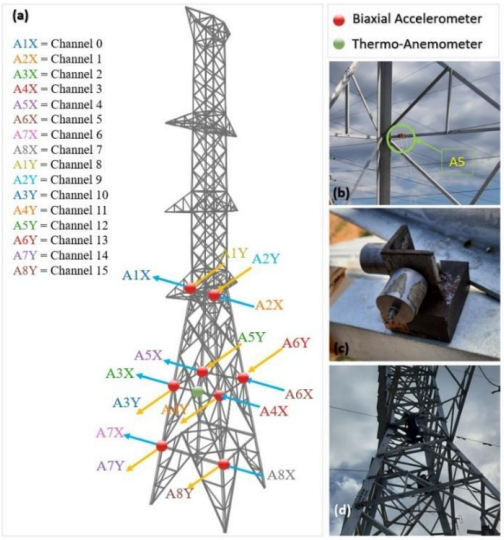


***Figure 2.*** (a) Location of sensors; (b) sensor A5 mounted on top of the tower member; (c) orientation of sensor; (d) placement of the sensor.

Due to safety constraints and limited accessibility, sensors were mounted only on the lower portion of the tower. Consequently, while modal frequencies and damping ratios could be analyzed, a complete reconstruction of mode shapes was not feasible. Figure 2a presents the specific locations of the sensors, while Figures 2b–2d provide close-up views of sensor A5, showcasing its placement and orientation. The accelerometers were installed in two horizontal directions (x and y) to capture bidirectional vibrations. Data acquisition was performed at a sampling rate of 40 Hz to focus on frequency components below 20 Hz, following the Nyquist criterion.

The recorded data are immediately organized and categorized. A total of 24 ten-minute datasets are evaluated and cleansed, and signal filtering is applied using the Butterworth filter

to isolate frequencies that are pertinent to the structural characteristics of the electrical transmission towers. The Butterworth filter's cutoff frequency is set at 2 Hz minimum and maximum of 19 Hz. Singular Value Decomposition (SVD) is applied to the Power Spectral Density (PSD) graphs to further refine the data.

## III. ML-BASED SSI

The SSI-COV algorithm [51] is the primary modal analysis method used in this study to identify modal parameters from covariance matrices of ambient vibration measurements. Its discrete-time state-space form is expressed as:

$$x_{r+1} = Ax_r + v_r$$
$$y_r = Cx_r + w_r \quad \text{(1a-1b)}$$

Where:
$x_r \epsilon \mathbb{R}^n$ : State vector at sample $r$ , $y_r \epsilon \mathbb{R}^l$ : Output vector at sample $r$ , $\boldsymbol{A} \epsilon \mathbb{R}^{n \times n}$: State transition matrix , $\boldsymbol{C} \epsilon \mathbb{R}^{n \times n}$: Observation matrix , $v_r$ : Process noise, $w_r$ : Measurement noise
$l$ : Number of monitored degrees of freedom (DOFs), $n$ : System order

Following the approach of Rosso et al. [30] and Cucuzza et al. [31], a Quasi-Monte Carlo (QMC) technique is adopted to automate the SSI process and avoid manual tuning of control parameters. Parameter sampling is performed using the Halton technique [53,54], and their limits are defined by Equations (2a–2d):

$$n \epsilon [n_{min}, n_{max}] = [2 \cdot l, i_{max} \cdot l]$$

$$j \epsilon [j_{min}, j_{max}] = \left[ \left| \frac{2}{max\{f_f, 1\}} \right|, j_{max} \cdot l \right]$$

$$t \epsilon [t_{min}, t_{max}] = [0, j_{max}]$$

$$i \epsilon [i_{min}, i_{max}] = \left[ \left[ \frac{f_s}{2max\{f_f, 1\}} \right], 10 \left[ \frac{f_s}{2max\{f_f, 1\}} \right] \right] \quad \text{(2a-2d)}$$

To filter out only the stable poles, stability criteria [52] are applied as shown in Equations 3a- 3d:

$$\Delta f = \frac{f_a - f_b}{f_a} \leq 0.01$$

$$\Delta \xi = \frac{\xi_a - \xi_b}{\xi_b} \leq 0.05$$

$$1 - MAC(\Psi_a, \Psi_b) \leq 0.02$$
$$\xi_a \leq 0.10 \quad \text{(3a-3d)}$$

The extraction of physical poles from possibly stable poles is accomplished via Kernel Density Estimation (KDE), which predicts the frequency value where most poles coincide. The univariate KDE based on a Gaussian Kernel [37,55] is represented by Equations 4a-4b.

$$\phi = \frac{1}{N_p h}\sum_{p=1}^{N_p} K\left(\frac{z - z_p}{h}\right),$$

$$K\left(\frac{z-z_p}{h}\right) = \frac{1}{\sqrt{2\pi h}} e^{\frac{(z-z_p)^2}{2h}} \quad \text{(4a-4b)}$$

where $\hat{\phi}$: estimated probability density function (PDF) obtained from the KDE
$h$ : bandwidth or smoothing parameter (fixed for all samples)
$N_p$ : all possible stable poles

Phase 1 involves generating quasi-random sets of control parameters using the Halton technique and conducting a minimum of 100 useful QMC simulations [32], analyzing their stabilization diagrams through KDE, and training an ML model to classify feasible parameter sets based on an Information Content (IC) index of 0.01. Phase 2 then automates the identification of physical modes by filtering only high-quality simulations using the information obtained from Phase 1.

The selection of KNN, DT, and XG in this study is based on their established roles in ML-based SHM, particularly in modal parameter identification. KNN [49] is convenient and widely used; however, it struggles with computational efficiency and is sensitive to data quality and hyperparameter choices. DT [6, 38] strikes a balance between ease of use and performance, but caution must be taken to mitigate overfitting and sensitivity to the data. Meanwhile, XG, an open-source machine learning package introduced by Chen and Guestrin [50], has gained significant popularity due to its high performance in regression, classification, and ranking tasks.

Relationships between mode shape matrices of selected nodes from both the FI and PV stages are presented both numerically and visually. The Modal Assurance Criterion (MAC) [17], a statistical correlation criterion as shown in Equation 5.

$$MAC(\psi_{PV}, \psi_{FI}) = \frac{\left|(\{\psi_{PV}\}^T\{\psi_{FI}\})\right|^2}{(\{\psi_{PV}\}^T\{\psi_{PV}\})(\{\psi_{FI}\}^T\{\psi_{FI}\})} \quad (5)$$

where $\psi_{PV}, \psi_{FI}$ are the analytical and operational mode shape vectors, respectively.

## IV. ML MODEL PERFORMANCE & MODAL ANALYSIS

*4.1 PV Stage*

A minimum of 100 useful sets and a study-defined maximum of 650 feasible sets were simulated across all ML models to estimate modal parameters with minimal deviations. Table

1 presents the effectiveness of each ML model in extracting useful sets during both phases. RF and XG demonstrated the highest efficiency, achieving 100% accuracy while requiring fewer sampled sets—260 and 272, respectively. In contrast, KNN and DT required significantly more sampled sets—355 and 338, respectively—to achieve 85% and 92% accuracy. These results suggest that KNN and DT require larger datasets to reach optimal performance.

***Table 1.*** ML models' evaluation report – PV stage.

| | Phase 1 | | | Phase 2 | | |
|---|---|---|---|---|---|---|
| **ML Model** | **Runtime (hrs)** | **TS[1]** | **Accuracy[2]** | **Runtime (hrs)** | **TS[1]** | **Accuracy[2]** |
| RF | 1.71 | 260 | 100% | 1.53 | 1911 | 100% |
| XG | 1.84 | 272 | 100% | 1.63 | 2022 | 100% |
| KNN | 1.92 | 355 | 85% | 1.76 | 2445 | 84% |
| DT | 1.73 | 338 | 92% | 1.68 | 2378 | 86% |

[1]Total Sampled Sets, [2]Obtained from Python Classification Report

For Phase 2, RF and XG maintain their accuracy at 100%, confirming their excellent generalization capability. However, DT experiences a decrease in accuracy from 92% in Phase 1 to 86% in Phase 2, indicating reduced reliability in predicting new parameter sets. Similarly, KNN drops from 85% to 84%. The faster runtime in Phase 2 across all models can be attributed to the elimination of the need to re-run the entire SSI process for each simulation. Instead, the trained ML models directly evaluate new parameter sets, streamlining the computational load. The extended runtime for KNN and DT remains notable, likely due to their exhaustive comparison-based nature, which requires analyzing a larger number of sets before achieving convergence. Thus, RF and XG prove to be the most efficient in selecting and discarding feasible sets, making them optimal choices for ML-based SSI.

Figure 3a presents the monitored acceleration data responses of the analytical model, showing clean acceleration signals due to the absence of environmental noise. Figure 3b presents the SVD of PSD, highlighting the fundamental frequencies of the first two bending modes, which peak at approximately 3.19 Hz and 3.23 Hz, respectively.

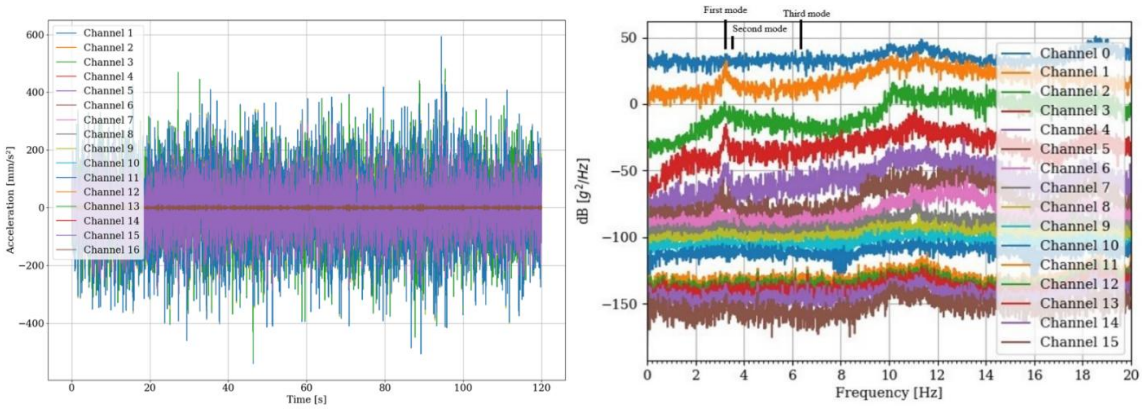


(a) (b)

***Figure 3.*** (a) PV stage's monitored signals and (b) SVD of PSD plot.

Figure 4 presents the overlapped SDs from the PV stage, illustrating the distribution of stable and unstable poles across multiple iterations of the QMC simulation. The diagram provides insight into mode stability, with selected poles representing modes that satisfy stability criteria for frequency, damping, and mode shapes. Poles labeled as "0" (red circles) indicate unstable modes that fail the stability conditions [30, 31].

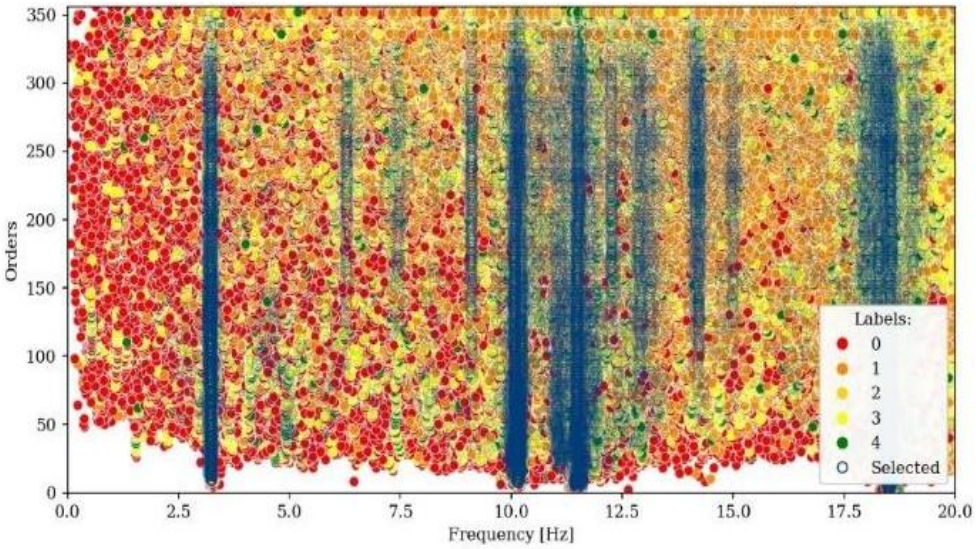


***Figure 4.*** PV stage's overlapped stabilization diagram after QMC simulations.

Figure 5 further refines the modal identification process by applying KDE to extract the most prominent modes. The KDE graph highlights that Mode 2 exhibits the highest density, making it the most identifiable mode, whereas Mode 1, despite being closely related, has a slightly lower KDE prominence. Local modes, such as Modes 3 and 4, are the least identifiable due to their lower modal participation. The KDE distribution also reveals significant modal activity within the 10 Hz–15 Hz frequency range, with additional peaks beyond 15 Hz, indicating the presence of higher-order modes.

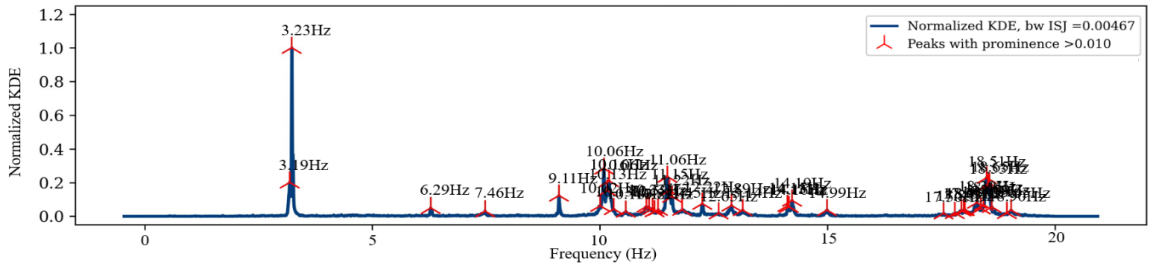


***Figure 5.*** Stable poles KDE along frequency – PV stage.

Tables 2 and A1 present the modal parameters estimated using ML-based SSI, SSI-BA, and NExT-ERA techniques. Based on mode shape characteristics and modal direction factors, five modes are classified as bending, three as torsional, and two as local. It is important to note that this modal classification is derived from the analytical model. The classifications are supported by visual inspection of the FEM-derived displacement vectors shown in Figure A1, which clearly illustrate the distinct global deformation patterns associated with each mode. Notably, Modes 3 and 4 exhibit localized displacements concentrated in the lower section of the tower. This behavior aligns with findings by Bhowmik and Chakraborti [11], who identified similar localized modal responses in a 34-meter transmission tower analyzed using STAAD Pro.

***Table 2.*** Identified modal frequencies – PV Stage.

| Mode | $f\ (Hz)$ | | | | | | | Category |
|---|---|---|---|---|---|---|---|---|
| | ML-Based SSI | | | | FEM | SSI-BA | NExT-ERA | |
| | RF | XG | KNN | DT | | | | |
| 1 | 3.187 | 3.189 | 3.186 | 3.188 | 3.217 | 3.193 | 3.234 | Bending |
| 2 | 3.230 | 3.231 | 3.231 | 3.231 | 3.236 | 3.227 | 3.247 | Bending |
| 3 | 6.286 | 6.289 | 6.280 | 6.288 | 6.301 | 6.246 | 6.173 | Local |
| 4 | 7.461 | 7.481 | 7.472 | 7.477 | 7.453 | 7.519 | 7.164 | Local |
| 5 | 9.109 | 9.095 | 9.098 | 9.109 | 9.114 | 9.027 | 9.375 | Torsion |
| 6 | 10.065 | 10.099 | 10.100 | 10.090 | 10.06 | 10.151 | 10.058 | Bending |
| 7 | 11.056 | 11.054 | 11.057 | 11.063 | 11.004 | 11.072 | 11.054 | Bending |
| 8 | 11.154 | 11.164 | 11.451 | 11.442 | 11.185 | 11.217 | 11.232 | Bending |

| | | | | | | | | |
|---|---|---|---|---|---|---|---|---|
| 9 | 12.220 | 12.242 | 12.280 | 12.250 | 12.233 | 12.256 | 12.2919 | Torsion |
| 10 | 14.192 | 14.149 | 14.181 | 14.179 | 14.191 | 14.202 | 14.213 | Torsion |

*4.2 FI Stage*

Table 3 presents the effectiveness of each ML model in extracting useful sets during both phases. The performance of ML models for both PV and FI stages follows almost similar patterns. There is a slight difference in the runtime of the FI stage compared to the PV stage dataset. The longer runtimes for KNN and DT—2.11 and 1.91 hours, respectively—are primarily due to the larger number of samples required to meet the convergence criteria, which impacts their overall efficiency.

Figure 6a presents the selected two-minute time history captured at eight locations along two axes. After Butterworth filtering, the SVD of PSD is developed and shown in Figure 6b.

***Table 3.*** ML models' evaluation report – FI Stage.

| | **Phase 1** | | | **Phase 2** | | |
|---|---|---|---|---|---|---|
| **ML Model** | **Runtime (hrs)** | **TS[1]** | **Accuracy[2]** | **Runtime (hrs)** | **TS[1]** | **Accuracy[2]** |
| RF | 1.92 | 290 | 98% | 1.74 | 2078 | 98% |
| XG | 2.01 | 301 | 98% | 1.86 | 2188 | 98% |
| KNN | 2.25 | 333 | 88% | 2.11 | 2578 | 84% |
| DT | 2.13 | 345 | 91% | 1.91 | 2523 | 85% |

[1]Total Sampled Sets, [2]Obtained from Python Classification Report

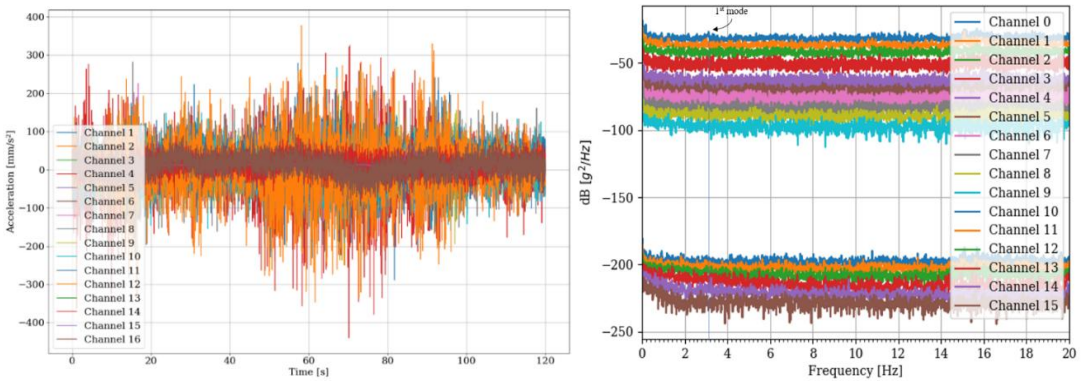


(a) (b)

***Figure 6.*** (a) FI stage's monitored signals and (b) SVD of PSD plot.

Comparing the overlapped SDs from Figures 4 and 7, the analytical vibration data clearly show distinct modal peaks, which are more easily distinguishable than those from field vibration data. These differences are anticipated due to the randomness of data from field tests, affected by the quality of testing owing to the limited number of sensors, and measurements are only conducted at the lower half of the structure.

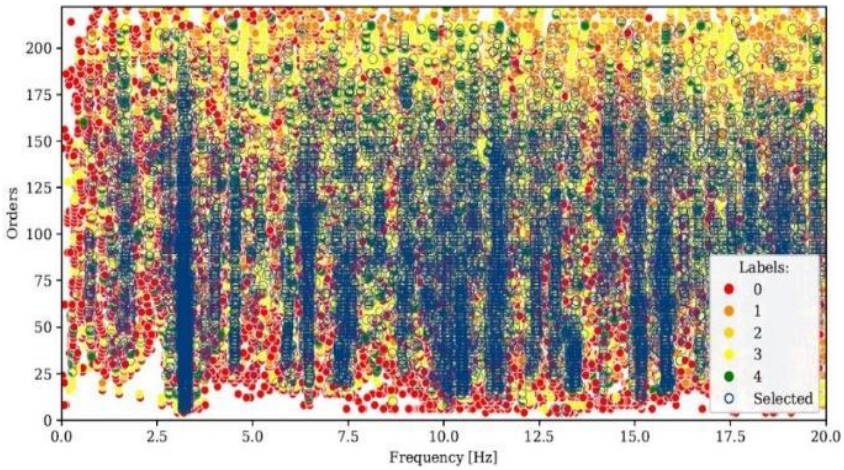


***Figure 7.*** FI stage's overlapped stabilization diagram after QMC simulations.

Figure 8 illustrates the KDE graph displaying all identified poles, accompanied by numerical values of selected frequencies from Table 4, and offers a visualization similar to a power spectral plot. The graph reveals the presence of numerous identified modes, even through automated modal analysis. This highlights that the quality of modal identification is highly dependent on the clarity and informativeness of the vibration data collected from the field.

The first and second modes are very identifiable but are located very close to each other, illustrating the challenge of distinguishing closely spaced modes, especially in structures with symmetrical cross-sections. Although we consider OMA as more representative of reality compared to numerical approximation, uncertainties and other factors related to field vibration collection affect the overall reliability of the OMA results. Given these uncertainties, we deliberately select only the modes that precisely match the numerical approximations to ensure a robust and unequivocal comparison of values and mode shapes between analytical and operational data.

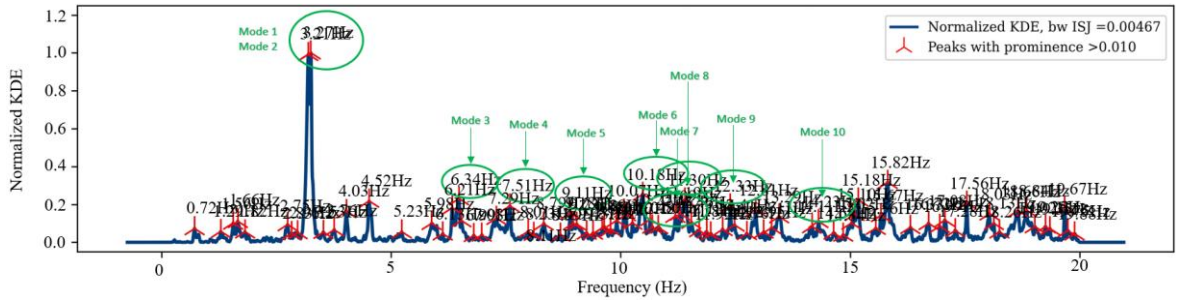


***Figure 8.*** Stable poles KDE along frequency – FI stage.

Despite the proven capability of automated SSI to detect the most prominent modes, there remains difficulty in extracting modes during the FI stage due to not fully informative vibration data. Table 4 and Figure 8 both illustrate the modal matching conducted in this study, based on the highest KDE values for the identified modes, where the highlighted frequency value is the selected modal frequency for the FI stage.

***Table 4.*** Selection of representative modes based on KDE.

| Mode | Frequency Value | KDE | Mode | Frequency Value | KDE |
|---|---|---|---|---|---|
| 3 | **6.34** | 0.22 | 8 | **11.30** | 0.21 |
| | 6.21 | 0.18 | | 11.32 | 0.08 |
| 4 | **7.51** | 0.18 | 9 | **12.33** | 0.3 |
| | 7.29 | 0.14 | | 12.81 | 0.17 |
| 5 | **9.11** | 0.17 | 10 | **14.23** | 0.09 |
| | 9.21 | 0.10 | | 14.11 | 0.08 |

Tables 5 and A2 present the modal identification results obtained from field measurements using ML models, alongside comparisons with conventional system identification methods. Notably, several modes—particularly Modes 6 and 9—are marked with NI (Not Identified) or NA (Not Applicable). This omission underscores the difficulty of extracting reliable damping information from low-excitation, noise-polluted ambient vibration data using conventional techniques. These methods often fail to detect weaker modes due to insufficient energy content or sensor limitations, resulting in incomplete or inaccurate damping estimations. Moreover, when damping ratios are identified, traditional approaches tend to yield higher values than ML-based results, which suggests a potential overestimation influenced by signal noise and reduced sensitivity to subtle vibrational responses.

Unlike damping, no specific code requirements exist for modal frequency values to limit vibrations and ensure structural integrity of the latticed tower. Consequently, a comparative analysis with similar studies remains the most reliable validation approach. The first fundamental frequency, identified at 3.21 Hz for a 38-meter tower, aligns well with expected values based on height-dependent trends observed in previous studies [3, 25, 26, 27, 28, 39]. This further substantiates the expected correlation between tower height and the first and second bending mode frequencies, as illustrated in Figure 9. The trend highlights a fundamental principle in structural dynamics: as tower height increases, structural flexibility generally increases and natural frequencies decrease, underscoring the importance of evaluating frequency behavior across varying tower configurations.

A notable general trend for transmission towers is the decrease in damping ratio values from lower to higher modes, similar to the modal results of Takeuchi et al. [40]. However, this does not necessarily occur in other structures, as variations can be specific to individual cases. It is understood in structural analysis that lower modes typically have the highest participation ratios; however, the relationship between damping ratios and modes is not fixed, and variations can occur due to several factors at different modes, as seen in the study of Feng et al. [28].

***Table 5.*** Identified modal frequencies – FI Stage.

| Mode | $f\ (Hz)$ | | | | | | |
|---|---|---|---|---|---|---|---|
| | ML-Based SSI | | | | | | NExT-ERA |
| | RF | XG | KNN | DT | FEM | SSI-BA | |
| 1 | 3.208 | 3.209 | 3.204 | 3.204 | 3.217 | 3.237 | 3.267 |
| 2 | 3.267 | 3.284 | 3.316 | 3.285 | 3.236 | 3.480 | 3.339 |
| 3 | 6.345 | 6.344 | 6.349 | 6.348 | 6.301 | 6.498 | 6.449 |
| 4 | 7.502 | 7.502 | 7.493 | 7.497 | 7.553 | 7.317 | 7.306 |
| 5 | 9.118 | 9.138 | 9.141 | 9.149 | 9.114 | 9.192 | 10.087 |
| 6 | 10.181 | 10.198 | 10.226 | 10.208 | 10.06 | NI[1] | NI |
| 7 | 11.091 | 11.071 | 11.062 | 11.012 | 11.004 | 11.836 | 11.491 |
| 8 | 11.301 | 11.326 | 11.325 | 11.336 | 11.185 | 12.368 | 12.048 |
| 9 | 12.334 | 12.399 | 12.395 | 12.406 | 12.233 | NI | NI |
| 10 | 14.234 | 14.236 | 14.229 | 14.228 | 14.429 | 18.225 | 18.336 |

[1]NI - Not Identified

According to the extracted damping ratio values for the first and second sway modes, even with aerodynamic damping effects neglected, the identified damping values of 3.02% and 2.51% remain below the ASCE 74 [42] recommendation of 4% and fall within the ranges specified by other international standards [41,43,44,45,46], which typically span from 1% to 8%. A study conducted by Zou et al. [3] on a 28-meter transmission tower in China during Typhoon Haima (Typhoon Lawin in the Philippines) recorded damping values of 2.84% (transverse direction) and 3.83% (longitudinal direction) under a 16 m/s mean wind speed, demonstrating that the damping ratios obtained in this experiment align with those observed in

full-scale structures subjected to extreme excitations.

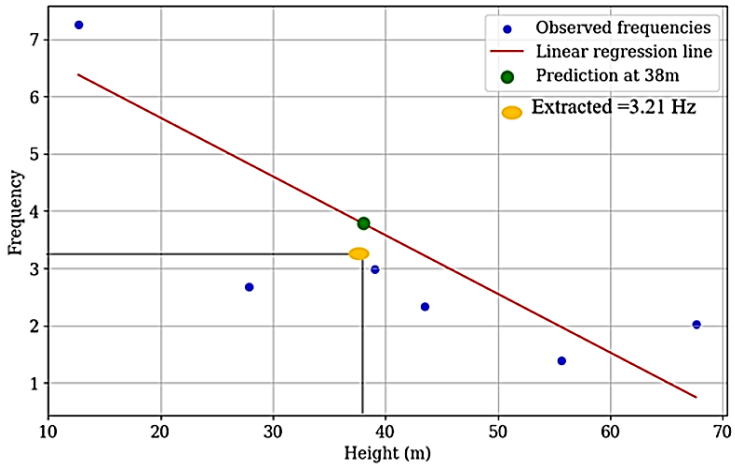


***Figure 9.*** Prediction vs estimated frequency value of the first mode.

Zhu et al. [39] highlighted that a higher damping ratio improves energy dissipation and reduces wind-induced oscillations, while a lower damping ratio necessitates increased tower mass and axial force capacity to maintain wind resistance. In this study, if the measured damping ratio is 3.02% but needs to be increased to 4%, retrofitting strategies should focus on enhancing energy dissipation mechanisms through structural modifications, such as adding or improving joint connections or incorporating high-damping materials, to effectively mitigate oscillations without significantly increasing structural mass. However, several factors may influence the accuracy of damping ratio estimations, including sensor precision, data acquisition quality, environmental variability, and nonlinear noise interference in the vibration signals. These uncertainties emphasize the importance of high-quality sensor deployment and improved signal processing techniques to enhance the reliability of damping estimations in transmission towers.

*4.3 PV Stage vs FI Stage*

Referring to Table 6, both RF and XG models maintained high accuracy during the PV stage, with 100% accuracy, but this value dropped to a decent 98% for both training and prediction. This decline can be attributed to the more random dataset that resulted in less identifiable modal peaks. Aside from DT, in the FI stage, KNN also exhibits a notable drop in accuracy from 88% in the training phase to 84% in the prediction phase. Despite this, there is no significant change in overall accuracy across different stages, which could be due to the stability of the dataset. As a result, overfitting analysis for these models is challenging to conclude definitively for this study.

Table 7 outlines the modal results obtained from two stages using the RF model: the PV stage, derived from the analytical model, and the FI stage, based on field sensor measurements. The percent change values indicate how much the frequencies have shifted from the PV to the FI stage. The frequencies shown here are selected from four models that exhibit the smallest relative differences from the FEM for both PV and FI stages. The frequency values recorded during the FI stage correspond well with those predicted by the theoretical model, with percent differences ranging from 0.11% to 1.25%, with the largest

increases observed in Modes 2, 6, and 8, and the smallest in Modes 5 and 10. Notably, all frequencies identified during the FI stage are slightly higher than their PV counterparts, except for Mode 7, which showed a marginal decrease of 0.54%. This may suggest that the analytical model's assumptions and estimations do not fully capture the tower's true dynamic responses. The assumption that the FEM model as the healthy state is not reasonable, however, values observe in the recent operational modal analysis serve as the baseline for future observation.

***Table 6***. Accuracy of each ML model - PV vs FI.

| | **Phase 1** | | **Phase 2** | |
|---|---|---|---|---|
| **ML Model** | **PV Accuracy** | **FI Accuracy** | **PV Accuracy** | **FI Accuracy** |
| RF | 100% | 98% | 100% | 98% |
| XG | 100% | 98% | 100% | 98% |
| KNN | 85% | 88% | 84% | 84% |
| DT | 92% | 91% | 86% | 85% |

For the damping ratios, significant discrepancies are observed, with percent changes ranging from –52.45% to +137.80%. These differences are expected because the FEM assumes a fixed damping ratio of 1% for all modes. Therefore, the damping values identified during the PV stage should cluster around this baseline. In contrast, the damping ratios obtained from the FI stage reflect the actual energy dissipation behavior of the structure under ambient conditions, which can vary due to material properties, joint flexibility, wind interaction, and other environmental factors. This contrast highlights the importance of field-based modal identification in refining model assumptions and enhancing the realism of structural simulations.

***Table 7.*** Modal parameter results– PV vs FI Stage

| Mode | $f\ (Hz)$ | | Percent Change[1] | $\xi$ (%) | | Percent Change |
|---|---|---|---|---|---|---|
| | PV | FI | | PV | FI | |
| 1 | 3.19 | 3.21 | 0.63 | 1.27 | 3.02 | 137.80 |
| 2 | 3.23 | 3.27 | 1.24 | 1.08 | 2.51 | 132.41 |
| 3 | 6.29 | 6.35 | 0.95 | 2.01 | 1.57 | -21.89 |
| 4 | 7.46 | 7.50 | 0.54 | 2.22 | 1.69 | -23.87 |
| 5 | 9.11 | 9.12 | 0.11 | 1.55 | 0.85 | -45.16 |
| 6 | 10.06 | 10.18 | 1.19 | 1.32 | 1.44 | 9.09 |
| 7 | 11.15 | 11.09 | -0.54 | 1.23 | 1.82 | 47.97 |
| 8 | 11.16 | 11.30 | 1.25 | 1.78 | 1.94 | 8.99 |
| 9 | 12.22 | 12.33 | 0.90 | 1.69 | 0.82 | -51.48 |
| 10 | 14.19 | 14.23 | 0.28 | 1.43 | 0.68 | -52.45 |

[1] $Percent\ Change = (FI - PV)/PV$

*4.4 Mode Shape Analysis and FE Model Updating*

Figure A1 presents the mode shapes derived from the ETABS model, serving as the reference for mode classification into bending, torsional, and local modes. Due to limited sensor placement on the lower portion of the tower, a complete reconstruction of mode shapes from field data was not possible. However, ML-based SSI was still able to estimate mode shapes, with only six frontal nodes considered for visualization in this study.

The sensor placement significantly influences mode shape accuracy, particularly for torsional modes, which require diagonal sensor positioning. Sensors were installed at three heights only and in two horizontal directions, limiting nodal coverage. As a result, higher-order bending and torsional modes (Modes 8, 9, and 10) were not fully identified, leading to lower MAC values for these modes.

The FI model was tuned to include operational damping ratios extracted from modal analysis, diverging from the original assumption ξ=1% for all modes as suggested by the Chinese GB50009-2012 Code for latticed towers and ξ=4% based on the ASCE standard. The model update utilized time history functions generated using a random wind noise vibration

using MATLAB (Scenario 1) and historical earthquake data from the 1940 El Centro earthquake (Scenario 2). As expected, from Figures A2-A4, the tower with a 1% damping ratio experiences the largest displacement, highest nodal shear, and overturning moment, highlighting the importance of accurate assumptions to avoid overdesign or under design.

*4.5 Variability Analysis*

For variability analysis, the 4-hour continuously monitored data is divided into 120 two-minute datasets. Each dataset undergoes individual ML-based SSI for each model. These tests were conducted over a short span of four hours in a single day, which may account for the stable temperature readings that varied between 29°C to 33 °C and the wind speeds that peaked at a modest 2 m/s.

Figure 10 shows the average values, including the standard deviations of performance scores from metrics across 120 runs of segmented datasets. From the representation, both RF and XG achieved high scores from different metrics such as accuracy, precision, recall, and F1-score—each maintaining 98-99% mean values in all categories. In contrast, KNN and DT exhibited lower performance levels. KNN scored ranging from 85 to 87, while DT displayed slightly higher precision at 86%, recall at 89%, F1-score at 87%, and accuracy at 88%. However, for smaller-scale applications with fewer sensors and datasets, DT's simpler structure offers a faster alternative. In light of these findings, this study highlights the importance of selecting and optimizing ML models based on specific data volumes and application requirements.

Figure A5 presents histograms and Coefficient of Variaton (CoV) values for 120 identified frequencies across ten modes of four ML-based SSI models, offering valuable insights into how the identification system responds to various types of different sets of acceleration data. The CoVs for frequencies show significant variation, ranging from 0.42% to 2.39%, suggesting that while the system is largely robust, some higher modes, like modes 9 and 10, display notable variability and also rank as the least identifiable. On the other hand, the CoVs for damping ratios, as shown in Figure A6, are significantly higher and more widely spread than those for frequencies, with values spanning from 2.02% to 7.02%.

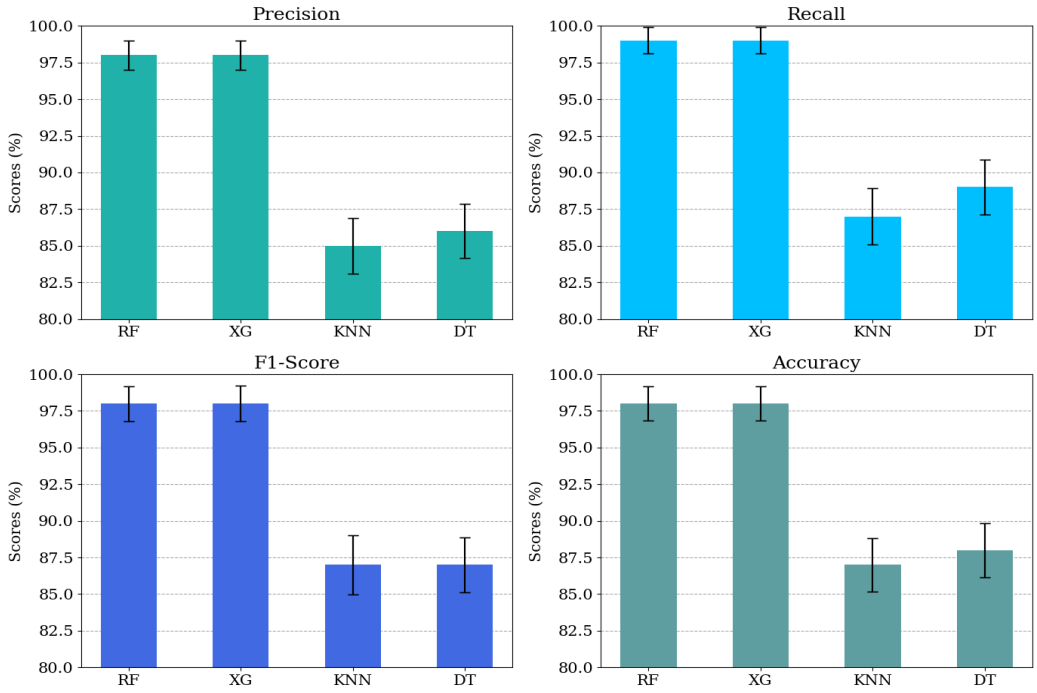


***Figure 10.*** Comparison of Phase 2 average score metrics for different ML models.

By inspecting Table 8, RF stands out, demonstrating the fastest processing time for 2-minute data intervals and considering sixteen sensor channels, higher accuracy in classifying stable modes, lower relative differences compared to analytical results, and smaller CoVs for random data sets. XG is also a strong contender, showing robust performance across multiple metrics. For simplicity, only the accuracy of the field test results is shown, as values for other evaluation metrics are very close to the accuracy values. Furthermore, correlation analysis using Pearson coefficients, such as for Mode 1 (see Figure A7), revealed weak and statistically insignificant relationships between modal frequencies and environmental variables like temperature and wind speed, and was therefore excluded in determining the best ML model, despite consistent readings across all models

***Table 8.*** Performance summary of ML models and best model selection based on key metrics.

| ML Model | Accuracy | Total Runtime (h) | Average Relative Difference (RD) vs FEM | | Average MAC (PV vs FI) | CoV | |
|---|---|---|---|---|---|---|---|
| | | | PV | FI | | f | $\xi$ |
| RF | 0.97 | 1.65 | 0.24 | 0.79 | 78.6 | 1.30 | 3.89 |
| XG | 0.96 | 1.86 | 0.30 | 0.93 | 78.6 | 1.32 | 3.94 |

| | | | | | | | |
|---|---|---|---|---|---|---|---|
| KNN | 0.89 | 2.33 | 0.38 | 1.09 | 78.2 | 1.38 | 4.04 |
| DT | 0.88 | 2.08 | 0.32 | 0.95 | 78.2 | 1.36 | 3.96 |

| **Metrics Evaluated** | Highest accuracy | Fastest runtime | Lowest RD | Highest average MAC | Lowest average CoV |
|---|---|---|---|---|---|
| **Best Performing Model** | RF/XG | RF | RF | RF/XG | RF |

## V. CONCLUSIONS AND RECOMMENDATION

Despite the challenges posed by limited sensor placement and environmental variability, this study establishes a strong foundation for developing an automated and comprehensive Structural Health Monitoring (SHM) system for transmission towers and other critical infrastructures in the Philippines. The successful implementation of Rosso et al.'s (2023) Stochastic Subspace Identification (SSI) algorithm demonstrates its viability in extracting dynamic characteristics from both digitally simulated and field-measured vibration data, making it an effective first-level damage detection tool. Expanding sensor deployment across higher elevations of the tower will enhance mode shape estimation, allowing for more precise damage localization. Future research should explore environmental variability, including nighttime measurements with fluctuating temperatures and higher wind speeds, to further validate the system's robustness.

The results confirm a strong alignment between operational modal analysis (OMA) and finite element model (FEM) predictions, though significant variability in many modes makes mode-matching challenging. While fundamental frequencies closely follow theoretical expectations, damping ratios exhibit greater uncertainty, with Mode 1 showing a deviation of up to 138%. These findings highlight the sensitivity of damping estimation to field conditions, emphasizing the need for high-quality data acquisition equipment and optimized sensor deployment.

Among the machine learning (ML) models tested, Random Forest (RF) outperformed other algorithms, delivering higher accuracy, faster processing times, and lower deviations from FEM results. XGBoost (XG) also demonstrated strong performance, whereas K-Nearest Neighbors (KNN) and Decision Trees (DT) exhibited longer runtimes and lower efficiency, suggesting the need for further optimization through Bayesian tuning or the exploration of alternative ML models.

To enable real-time monitoring of transmission towers, future studies should integrate more automated and noise-sensitive data acquisition and preprocessing systems capable of filtering and refining vibration signals before modal identification. This requires interdisciplinary collaboration, particularly with hardware specialists, to develop a data acquisition interface compatible with multiple sensor types, including accelerometers. Ultimately, this study serves as a stepping stone toward a fully automated SHM system, bridging the gap between real-time data collection and structural performance assessment, ensuring the resilience and safety of critical infrastructures in the Philippines.

## VI. ACKNOWLEDGEMENTS

The authors extend their sincerest gratitude to the Engineering Research and Development for Technology (ERDT) under the Department of Science and Technology (DOST) for financial support for the ongoing implementation of this work.

Special thanks are extended to Dr. Marco Martino Rosso (Politecnico di Torino, Italy) for granting permission to use the automated OMA tool and for generously explaining the algorithm.

The authors also thank PENELCO Bataan for permitting vibration tests on one of their towers, which significantly contributed to this research.

**References:**

[1] Aboshosha H, Elawady A, El Ansary A, El Damatty A. 2016. Review on dynamic and quasi-static buffeting response of transmission lines under synoptic and non-synoptic winds. Engineering Structures, 112:23-46.

[2] Fu X, Wang J, Li H, Li J, Yang L. 2019. Full-scale test and its numerical simulation of a transmission tower under extreme wind loads. Journal of Wind Engineering and Industrial Aerodynamics. 190:119-133.

[3] Zou Y, Lei X, Yan L, He X, Nie M, Xie W, Luo X. 2020. Full-scale measurements of wind structure and dynamic behaviour of a transmission tower during a typhoon. Structure and Infrastructure Engineering. 16(5):820-830.

[4] Albermani F, Kitipornchai S. 2003. Numerical Simulation of Structural Behaviour of Transmission Towers. Thin-Walled Structures.

[5] Karami-Mohammadi R, Mirtaheri M, Salkhordeh M, Hariri-Ardebili MA. 2020. Vibration anatomy and damage detection in power transmission towers with limited sensors. Sensors. 20(6):1731.

[6] Kouchaki M, Salkhordeh M, Mashayekhi M, Mirtaheri M, Amanollah H. 2023. Damage detection in power transmission towers using machine learning algorithms. Structures. 56.

[7] Wan J-W, Li Q-S, Han X-L, Xu K. 2022. Investigation of structural responses and dynamic characteristics of a supertall building during Typhoon Kompasu. Journal of Wind Engineering Industrial Aerodynamics. 230(9):105209.

[8] Wu C, Yang X, Zhang B, Liu Z, Zhao Y. 2021. Dynamic response of a cat head type transmission tower-line system under strong wind. Journal of Physics Conference Series 1986(1):012098

[9] Fu X, Li H-N, Li G, Dong Z-Q. 2020. Fragility analysis of a transmission tower under combined wind and rain loads. Journal of Wind Engineering Industrial Aerodynamics.

[10] AlHamaydeh M, Aswad NG. 2022. Structural health monitoring techniques and technologies for large-scale structures: Challenges, limitations, and recommendations. Practice Periodical on Structural Design and Construction. 27(3).
[11] Bhowmik C, Chakraborti P. 2020. Analytical and experimental modal analysis of electrical transmission tower to study the dynamic characteristics and behaviors. KSCE Journal of Civil Engineering. 24(3).
[12] Chang C-M, Loh C-H. 2015. Improved stochastic subspace system identification for structural health monitoring. 11th International Conference on Damage Assessment of Structures.
[13] García, KL, Maes K, Parnás VE, Lombaert G. 2021. Operational modal analysis of a self-supporting antenna mast. . Journal of Wind Engineering Industrial Aerodynamics. 209:104490.
[14] Zeferino J, Gonçalves E, Carapito P, Santos F. 2021. Monitoring system of an industrial steel tower structure. Lecture Notes in Civil Engineering, Civil Structural Health Monitoring-8 Workshop. Springer. 156: 499-506.
[15] Peeters B, De Roeck G. 2001. Stochastic system identification for operational modal analysis: A review. Journal of Dynamic Systems Measurement and Control. 123(4):659-667.
[16] Zahid FB, Ong C, Khoo S. 2020. A review of operational modal analysis techniques for in-service modal identification. Journal of the Brazilian Society of Mechanical Sciences and Engineering. 42(8).
[17] Allemang RJ, Brown DL. 1982. A correlation coefficient for modal vector analysis. 1st International Modal Analysis Conference; Orlando, USA. p. 110-116.
[18] Garcia-Macias E, Ubertini F. 2020. Automated operational modal analysis and ambient noise deconvolution interferometry for the full structural identification of historic towers: A case study of the Sciri Tower in Perugia, Italy. Engineering Structures. 215:110615.
[19] Li HN, Wang JX, Fu X, Ren L, Zhang Q. 2020. Field measurements of typhoon effects on a transmission tower and its modal parameter identification. Advances in Structural Engineering. 23(8).
[20] He YC, Li Z, Fu J, Wu JR, Ng CT. 2021. Enhancing the performance of stochastic subspace identification method via energy-oriented categorization of modal components. Engineering Structures.
[21] Mugnaini V, Zanotti Fragonara L, Civera M. 2022. A machine learning approach for automatic operational modal analysis. Mechanical Systems and Signal Processing. 170:108813.
[22] Zini G, Betti M, Bartoli G. 2022. A quality-based automated procedure for operational modal analysis. Mechanical Systems and Signal Processing. 164(1-2):108173.
[23] Tronci EM, De Angelis M, Betti R, Altomare V. 2022. Multi-stage semi-automated methodology for modal parameters estimation adopting parametric sys identification algorithms. Mechanical Systems and Signal Processing. 165(5):108317.
[24] Ardilla YV, Gomez-Araujo ID, Villalba-Morales JD. 2023. An automated procedure for continuous dynamic monitoring of structures: Theory and validation. Journal of Vibration Engineering & Technologies. 12(1).
[25] Li H-N, Wang J-X, Fu X, Ren L, Zhang Q. 2020. Field measurements of typhoon effects on a transmission tower and its modal parameter identification. Advances in Structural Engineering. 27(2).
[26] Hsu T-Y, Chien C-C, Shiao S-Y, Chen C-C, Chang K-C. 2020. Analysis of Environmental and Typhoon Effects on Modal Frequencies of a Power Transmission Tower. Sensors. 20(18).
[27] Xingjie W, Tingting Y, Meigen C, Chong Z, Wensong Z, Yutong, P. 2021. Damage Detection of Transmission Tower Based on Stochastic Subspace and Statistic Model. IOP Conference Series: Earth and Environmental Science. 687(1):012086.
[28] Feng Y, Su Y, Zhao C, Zhu Y, Sun Q. 2024. A two-stage automated OMA framework for transmission towers based on clustering algorithms. Structures. 61(106023).
[29] Zhou K, Li Q-S, Han X-L. 2022. Modal identification of civil structures via stochastic subspace algorithm with Monte Carlo–based stabilization diagram. Journal of Structural Engineering. 148(6).
[30] Rosso MM, Aloisio A, Parol J, Marano GC, Quaranta G. 2023. Intelligent automatic operational modal analysis. Mechanical Systems and Signal Processing. 201:110669.
[31] Cucuzza R, Aloisio A, Civera M, Ricciardi G, Domaneschi M. 2024. Dynamic characterization and FE model updating via metaheuristic algorithm of two confined masonry buildings. Engineering Structures. 308:117935.
[32] Zhou K, Xie D-L, Xu K, Zhi L-H, Hu F, Shu Z-R. 2023. A machine learning-based stochastic subspace approach for operational modal analysis of civil structures. Journal of Building Engineering. 76:107187.
[33] Brincker R, Zhang L, Andersen P. 2000. Modal identification from ambient responses uing frequency domain decomposition. IMAC 18: International Modal Analysis Conference; Texas, USA.

[34] Caicedo, JM. 2011. Practical guidelines for the natural excitation technique (NExT) and the Eigensystem realization algorithm (ERA) for modal identification using ambient vibration. Experimental Techniques. 35:52-58.
[35] Farrar CR, Worden K. 2012. Structural health monitoring: A machine learning perspective. John Wiley & Sons, Ltd.
[36] Regni M, Arezzo D, Carbonari S, Gara F, Zonta D. 2018. Effect of environmental conditions on the modal response of a 10-story reinforced concrete tower. Shock and Vibration.
[37] Bishop CM. 2006. Pattern recognition and machine learning. New York, NY: Springer.
[38] Safavian SR, Landgrebe D. 1991. A survey of decision tree classifier methodology. IEEE Transactions on Systems, Man, and Cybernetics. 21:660-674.
[39] Zhu YM, Sun Q, Zhao C, Wei ST, Yin Y, Su YH. 2023. Operational modal analysis of two typical UHV transmission towers: A comparative study by fast Bayesian FFT method. Engineering Structures 277.(4).
[40] Takeuchi M, Maeda J, Ishida N. 2010. Aerodynamic damping properties of two transmission towers estimated by combining several identification methods. Journal of Wind Engineering and Industrial Aerodynamics. 98:872-880.
[41] GB5009-2012. Load code for the design of building structures: China Architecture & Building Press.
[42] American Society of Civil Engineers. 2020. ASCE MOP 74: Guidelines for electrical transmission line structural loading. New York, NY.
[43] AS/NZS. 2011. Structural design actions, part 2: wind actions. Sydney, Australia.
[44] European Committee for Standardization. 2005. EN1991-1-4: Eurocode 1: Actions on Structures - Part 1-4: General Actions - Wind Actions.
[45] Standard B. BS 8100 Lattice Towers and Masts. British Standards Institution. 1986; 85.
[46] Society JE. Design Standard on structures for transmission. JEC-127-1979; 1979.
[47] Rokach L, Maimon O. 2014. Data mining with decision trees: Theory and applications. 2nd ed. World Scientific.
[48] Mostafaei H, Mostofinejad D, Ghamami M, Wu C. 2023. A new approach of ensemble learning in fully automated identification of structural modal parameters of concrete gravity dams: A case study of the Koyna dam. Structures. 50(2):255-271.
[49] Shelke P, Gole A, Kanherkar P, Singh S, Abhishek Pr. 2023. Comparative analysis of machine learning algorithms: Random forest algorithm, Naive Bayes Classifier, and KNN - A survey.
[50] Chen, T, Guestrin C. 2016. XGBoost: A scalable tree boosting system. 22nd ACM SIGKDD International Conference on Knowledge Discovery and Data Mining.
[51] Van Overschee P, De Moor B. 1993. Subspace algorithm for the stochastic identification problem. Automatica. 29(3):649-660.
[52] Rainieri C, Fabbrocino G. 2014. Operational modal analysis of civil engineering structures: An introduction and guide for applications. New York: Springer.
[53] Owen AB. 2017. A randomized Halton algorithm in R (Version 2) [Preprint]. arXiv.
[54] Hou T, Nuyens D, Roels S, Janssen H. 2019. Quasi-Monte Carlo-based uncertainty analysis: Sampling efficiency and error estimation in engineering applications. Reliability Engineering & System Safety 191(2-3):106549.
[55] Silverman BW. 1998. Density estimation for statistics and data analysis. The Kernel Method for Univariate Data. Chapman and Hall/CRC. p. 34-72,).